Capacity Optimization of Off-Grid Wind-Solar-Diesel-Battery System Based on Improved Whale Optimization Algorithm

Jia Lu[1,2*], Fei Lu Siaw[1*], Tzer Hwai Gilbert Thio[1], Junjie Wang[3], Dong Yang[4]

Abstract:

In the early stage of microgrid construction, reasonable allocation of power equipment capacity based on regional resource characteristics can not only effectively solve the power supply reliability problem caused by wind and solar uncertainty, but also improve the system's economy and environmental protection. This design constructs a off-grid wind-solar-diesel-storage microgrid, establishes a multiobjective optimization model comprehensively considering costs of energy, carbon emissions, and the loss probability of power supply. The energy control strategy of the battery priority tracking load was adopted and the operating conditions of each part were analyzed under 8 working conditions based on net load and battery SOC status. After testing a series of intelligent optimization algorithms, the whale optimization algorithm was improved through adaptive t-distribution, dynamic selection strategy, and differential change strategy. By verifying and analyzing the data from a hospital complex in Montagu, California, USA, it is evident that the established model and control strategy can effectively meet the load demand and achieve the optimal equipment capacity ratio. The Improved Whale Optimization Algorithm (IWOA) demonstrates higher solution accuracy and faster convergence speed in optimization calculations.

Keywords: Capacity configuration, Metaheuristic optimization, Off-grid Microgrid, Wind-solar hybrid power system

1 Introduction

Energy serves as the fundamental material basis for human society. However, the conventional emission of significant amounts of greenhouse gases and pollutants from traditional energy sources is [1] increasingly contributing to global climate change.

1.Centre for Advanced Electrical and Electronic Systems (CAEES), Faculty of Engineering, Built Environment and Information Technology, SEGi University, 47810 Petaling Jaya, Selangor, Malaysia.

2.Department of Electronic Engineering, Taiyuan Institute of Technology, 030008, Taiyuan, Shanxi, China

3.Department of Production and Environmental Protection, China Huaneng Group CO., Ltd. Shandong Branch. 250014 Jinan, Shandong, China

Environmental pollution, in turn, presents a grave threat to both the natural ecological environment and human health. (Abdalla, et al., 2021; Bakeer, et al., 2023; Lian, et al., 2019; Shezan, et al., 2023). In the past 20 years, clean power generation technologies such as wind energy, ocean energy, solar energy, biomass energy, geothermal energy and nuclear energy have become the focus of widespread attention of governments, the scientific and technological communityand the public (Chen, et al., 2021; Kotb, et al., 2022). Wind and solar account for a record 12 % of the global electricity mix by 2022, up from 10% in 2021. Solar power generation grew 24%, making it the fastest-growing source of electricity for 18 years in a row. Wind power generation increased by 17% (Małgorzata Wiatros-Motyka, 2023).

Akikur, et al. (2013) found that single solar power systems are cost-effective, environmentally friendly, and easy to maintain for off-grid locations in rural areas, and the hybrid system can meet the load requirements better because the other source covers the weaknesses of one source. Akbas, et al. (2022) introduced optimal solution approaches for rural electrification, outlining four core issues: optimal system configuration and unit size, optimal power dispatch strategy, optimal technology selection, and optimal network design. Additionally, they presented potential avenues for further studies in rural electrification from an optimization standpoint. During the past two decades, microgrid planners have focused on optimization problems that are affected by significant overloads in computational methods. Finding practical techniques to correctly calculate microgrid capacity has been a key issue (Bukar, et al., 2020). In recent years, Zhao and Yuan (2016) proposed an improved fruit fly optimization algorithm to solve the problem of optimizing the power supply capacity of independent microgrids, the optimization objectives being the minimum annual total cost and pollutant emission of the system. The simulation results showed the excellent performance of the proposed optimization method. However, higher power supply reliability is not considered. Emad, et al. (2021) developed a mathematical model for a hybrid PV/wind/battery system, discussed different effects of the LPSP value on system COE, and finally found the best optimal system configuration using PSO, GWO, WHO, GA, and HOMER. Compared to the genetic algorithm (GA), the particle swarm algorithm (PSO), the whale optimizaiton algorithm (WOA), the wild horse optimizer (WHO), and the enhanced whale optimization algorithm (EWOA), (Liu, et al., 2022) proposed an improved whale optimization algorithm (IWOA) with lower integrated costs and higher operational efficiency. The result showed that the IWOA is better at solving the MG operations planning problem. Amupolo, et al. (2022) used HOMER software to study the deployment of solar home systems and microgrids in informal settlements in Namibia and found the optimal energy system by minimizing net current cost (NPC) and average cost of energy (LCOE). It also assesses the impact of changes in diesel prices, load demands, and solar PV module costs on the optimal energy system. Bakeer ,et al. (2023) proposed African Vulture Optimization method (AVOA) which considers the realization of the minimum energy cost and the probability of power loss. The results show that AVOA performs better in convergence and execution time. Dong, et al. (2021) developed a multi-

4.Shanxi Yinhe Electronics Equipment Plant, 030006 Taiyuan, Shanxi, China

*corresponding author: Jia Lu

objective optimization model, considering investment cost, environmental impact, and power supply quality. They enhanced the multi-objective sparrow search algorithm using niche optimization technology and incorporated the Levy flight strategy for improved optimization. Simulation results validate the efficacy of this enhanced algorithm in reducing redundancy and improving optimization outcomes.

This paper analyzes the output characteristics of individual micro-power sources and establishes an optimal microgrid configuration model that takes into account factors such as minimizing energy costs, carbon emissions, and the probability of power supply loss. An improved whale optimization algorithm (IWOA) is proposed using three improvement strategies, namely adaptive T-distribution, dynamic selection strategy, and differential variation strategy. Effectively improve the search accuracy and convergence speed of the optimizaiton.

2 Wind-solar-diesel-battery power generation system model

The typical structure of a hybrid wind-solar power generation system is shown in Figure 1. It mainly includes photovoltaic cells, wind turbines and other power generation equipment, batteries and diesel generators for the regulation and supplement of electric energy (Yoshida & Farzaneh, 2020)

Figure 1 Configuration of wind-solar-diesel-battery system

2.1 Wind power output model

Wind power generation is the main form of wind energy utilization, and the main component is the wind turbine. The output power is determined according to the wind speed, as indicated in the guidance manual, referring to the wind speed at the fan hub. This speed can be derived through conversion using Equation (1) (Zhao & Yuan, 2016):

$$\frac{v}{v_{ref}} = (\frac{H}{H_{ref}})^{\alpha}$$ (1)

Where, H is the height of the hub of the fan, it is 36m. H_{ref} is the standard height, it is 50m. v_{ref} is the standard wind speed, and the unit is m/s. α is the roughness of the surface, usually 0.3.

The output power can be obtained according to the wind-power curve (Chen ,et al., 2021):

$$P_{WT}(t) = \begin{cases} 0 & v(t) \le v_i, \quad v_p < v(t) \\ \eta_W P_{WTr} & v_i < v(t) < v_r \\ P_{WTr} & v_i < v(t) < v_p \end{cases} \tag{2}$$

$$\eta_W = \frac{v - v_i}{v_r - v} \tag{3}$$

Where $P_{WT}(t)$ is the real-time output power of the wind turbine, v_i is the start-up wind speed. v_r is the rated wind speed. v_p is the survival wind speed. η_W is the ratio of output power and the rated power. P_{WTr} indicates the rated power.

Wind output power can be obtained as following formula (4) (Chunhui Liang, 2023):

$$P_{WT} = N_i \cdot \left[\sum_{t=1}^{24} P_{WT}(t) \cdot t \right] \tag{4}$$

2.2 Photovoltaic power output model

Photovoltaic power generation is a method of converting solar energy directly into electricity through the use of solar panels. Solar panel output power P_{pv}, solar irradiation intensity E_{ac}, and ambient temperature are shown in Equation (5) (Aeidapu MAHESH, 2020):

$$P_{PV}(t) = P_{PVr} \frac{E_{ac}}{E_{STC}} \left[k \left(T(t) - T_{STC} + 30 \times \frac{E_{ac}}{E_{STC}} \right) + 1 \right] \tag{5}$$

Where P_{PVr} is the rated output power of solar panels under standard test conditions (25.0 °C, 1.0 MPa). E_{STC} is the light intensity under standard test conditions, and the value is 1 kW/m². E_{ac} is real light intensity. k is the power temperature coefficient, which is -0.47%/°C. T_{STC} is the test reference temperature, generally 25 °C. $T(t)$ is the Celsius temperature on the surface of the solar panel.

2.3 Energy storage battery equipment model

Storage batteries are adopted as the storage equipment that can balance supply and demand in the new energy generation in this paper. The relationship between SOC and charging and discharging is shown in (6-8) (Zhao, et al., 2023):

$$\begin{cases} P_{charge} = \eta_{charge} \left(P_{WT} + P_{PV} - P_{Load} \right) \\ P_{discharge} = \left(P_{Load} - P_{WT} - P_{PV} \right) / \eta_{discharge} \end{cases} \tag{6}$$

$$\begin{cases} SOC(t + T_S) = (1 - \delta) SOC(t) + P_{charge} T_S / E_{Bat}(t) \\ SOC(t + T_S) = (1 - \delta) SOC(t) - P_{discharge} T_S / E_{Bat}(t) \end{cases} \tag{7}$$

$$E_{Bat}(t) = E_{STC} \left[1 + \delta_b \left(T_c - T_{stc} \right) \right] \tag{8}$$

Where SOC(t+T_S) is the remaining power of the electric storage device at t+T_S time; T_S is time interval, taking 1 h; P_{charge}(t) is charge power at t time; $P_{discharge}$(t) is discharge power at t time; δ is self-discharge rate, T_S is the time interval, taking 1 h; t is any certain

time in one year.

2.4 Diesel generator model

The mathematical relationship between the operating power of diesel generators and the oil consumption is concerned with the capacity optimization configuration of microgrids. Referring to relevant literature, the output power of diesel generators with fuel consumption shows a linear relationship in Equation (9) (Das, et al., 2017; Zhao, et al., 2013):

$$F_{DG}(t) = c_{f1}P_{DGr} + c_{f2}P_{DG}(t) \tag{9}$$

Where, $F_{DG}(t)$ is the fuel consumption at t time, P_{DGr} is the rated power of the diesel generator. $P_{DG}(t)$ is the output power of the diesel generator. c_{f1} is the intercept coefficient of the diesel generator fuel curve, and c_{f2} is the slope of the diesel generator fuel curve. Unit is L/kW.

3. Control strategy and optimization objectives

3.1 Energy control strategy

A strategy based on diesel turn-on/off conditions is proposed, when wind power, photovoltaic power, and energy storage cannot meet the load requirements, or wind power, photovoltaic cannot meet the load requirements and energy storage reserves reach the lower limit at the same time, the diesel generators start up. When wind power, photovoltaic output, and energy storage can meet the load requirements and energy storage has a certain energy reserve, or the wind power and photovoltaic resources are sufficient, even if the diesel generators work at the minimum power, still leads to the maximum power of the energy storage charge, the diesel generator is shut down. The net load of the grid (P_{NL}), its value is the active power difference between the load electricity demand and the new energy power output.According to the value of SOC and P_{NL}, the operating conditions can be divided into the following eight states:

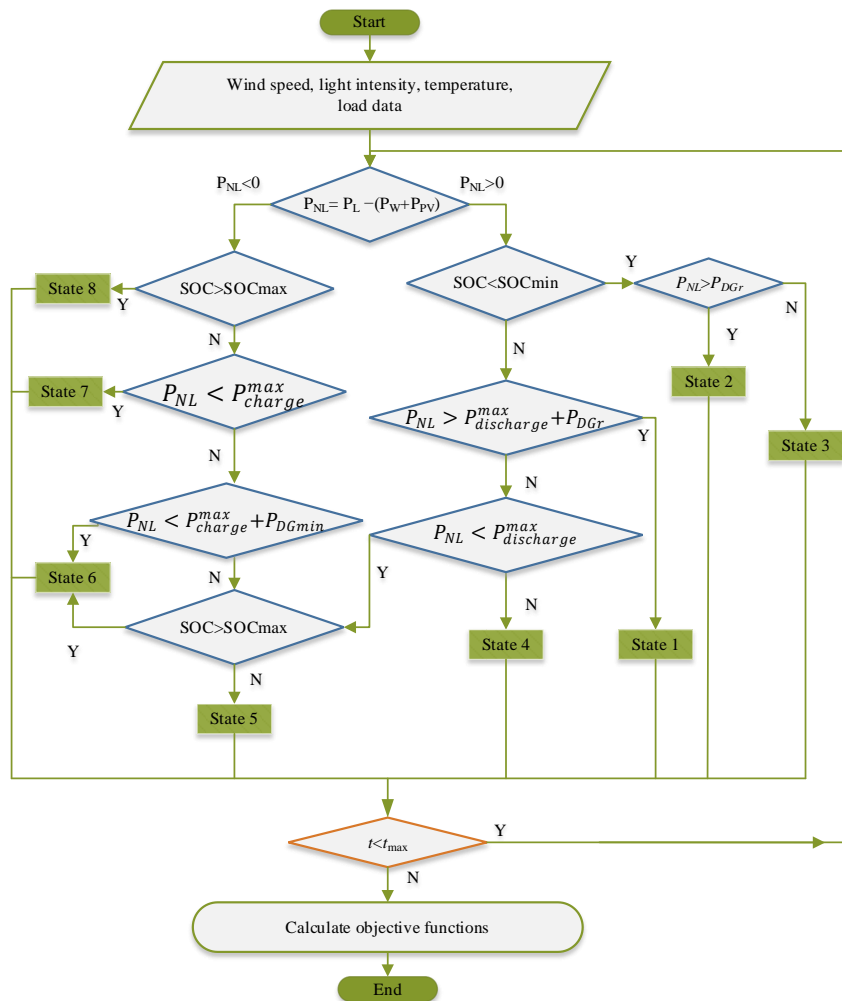The flow of the energy control strategy is shown in Figure 2:

Figure 2. Energy control strategy flow

According to the above 8 states, the working conditions of each equipment are shown in Table 1.

Table 1. Distributional generator working conditions in different states

	Wind turbine	Solar panel	Diesel generator	Battery storage	Load
1	Full load	Full load	Full load	Maximum power discharge	Cutting off some load
2	Full load	Full load	Full load	No charge or discharge	Cutting off some load
3	Full load	Full load	Tracking load	No charge or discharge	Being tracked
4	Full load	Full load	Tracking load	Maximum power Discharging	Being tracked
5	Full load	Full load	Tracking shutdown	Tracking load	Being tracked
6	Full load	Full load	Shutdown	Tracking load	Being tracked
7	Limited power output	Limited power output	Shutdown	Maximum power Charging	All be working

8	Limited power output	Limited power output	shutdown	No charge or discharge	All be working

3.2 Optimization objective

The optimization objective is to achieve the minimum cost, the highest reliability of the power supply, the highest utilization rate, and the minimum carbon emission of the integrated system under the condition that each power source of the wind-solar hybrid system meets the constraints (Liang, et al., 2023). The final result of optimization is to obtain the optimal combination of the number of fans N_W, solar panels N_{PV}, battery N_{Bat}, and the diesel engine N_{DG} under the premise of meeting the objective function(Zhao ,et al., 2013).

3.2.1 Economic evaluation index

Various cost factors were considered comprehensively, including equal cost, operating and maintenance cost, replacement cost, fuel cost of the diesel generator, etc. The calculation formula is shown in Equation (10):

$$C_1 = C_{Init} + C_{OM} \tag{10}$$

C_1 is the equivalent cost, C_{Init} is the initial installation cost, and C_{OM} is the operation and maintenance cost.

(1)   initial installation cost

The initial equipment investment refers to the initial installation cost required by the project, which is determined by the installed quantity of distributed power supply, the capacity of a single unit and the cost of the unit capacity. This is the largest and most direct part of all economic investment. Considering that some equipment has the value of recycling, the equipment depreciation factor is included in the initial investment, and the specific calculation formula is shown in Equation (11-13) (Rajanna & Saini, 2016) :

$$C_{Init} = \sum_{i=1}^{4} \left[\frac{r(1+r)^{l_i}}{(1+r)^{l_i} - 1} \cdot \frac{N_i C_i}{365 \cdot l_i} \right] \tag{11}$$

$$N_i = (N_{WT}, N_{PV}, N_{Bat}, N_{DG}) \tag{12}$$

$$C_i = (C_{WT}, C_{PV}, C_{Bat}, C_{DG}) \tag{13}$$

Where, i is the type of power supply equipment, including wind turbine, photovoltaic, battery, and diesel generator. N_i is the number of each power supply. C_i is the unit cost of each distributed power supply, the unit is yuan/set. r is the depreciation rate of the equipment, 8% in this paper. . l_i is the lifespan of the i-th device.

(2)   Operation and maintenance costs

Operation and maintenance costs consider fixed operating and maintenance costs, fuel costs, and energy storage replacement costs as in Equation (14):

$$C_{OM} = C_{OMFlx} + C_F + C_{Replace} \tag{14}$$

Where, C_{OM} is total operating and maintenance costs, C_{OMFix} is fixed operating and maintenance costs, C_F is fuel costs, and $C_{Replace}$ is replacement costs.

$$C_{OMFix} = \sum_{i=1}^{4} \left\{ \sum_{t=1}^{24} \left[\frac{N_i \cdot P_{ir}(t) \cdot c_{OMi}}{365 \cdot l_i} \right] \right\} \tag{15}$$

$$P_{ir} = (P_{WTr}, P_{PVr}, P_{Batr}, P_{DGr}) \tag{16}$$

$$c_{OMi} = (c_{OMWT}, c_{OMPV}, c_{OMBat}, c_{OMDG}) \tag{17}$$

Equations (15-17) are fixed operating and maintenance costs, which are determined by the number of distributed power units installed and the maintenance costs of the unit. Where, N_i is the number of each power supply. P_{ir} is the rated output of the i_{th} power. c_{OMi} is the maintenance cost coefficient of each power supply, and the unit is yuan /kWh.

$$F_{uel} = \sum_{t=1}^{24} \left[c_{f1} P_{DGr} + C_{f2} P_{DG}(t) \right] \tag{18}$$

$$C_F = F_{uel} \times U_{fuel} \tag{19}$$

In equations (18-19), F_{uel} is the total fuel consumption of the diesel generator within a typical day. C_F is the fuel cost. U_{fuel} is the unit price of diesel oil.

The present value of a system's replacement cost is the net present value of all replacement costs incurred over the lifetime of the system.

$$C_{Replace} = \sum_{i=1}^{4} \left[\sum_{t=1}^{24} N_i \cdot P_{ir}(t) \cdot c_{Ri} \right] \tag{20}$$

In equation (20), $C_{Replace}$ is the cost of replacing the equipment within a typical day.

c_{Ri} is the replacement cost of type i_{th} equipment.

3.2.2 Power distribution reliability

Reliability is a very important factor to estimate the effect of power outages on consumers, it can be calculated by equaition (21):

$$C_2 = c_{loss} \cdot \sum_{t=1}^{24} P_{loss}(t) \tag{21}$$

Where, C_2 is the penalty cost for cutting off part of the load in the microgrid. C_{loss} is the penalty unit price of load removal. $P_{loss}(t)$ is the power of the cutting load at time t.

Power supply reliability is reflected by the loss of power supply probability (LPSP), which is defined as the proportion of the system shortage load to the total power load of the system. In general, the LPSP value is between 0 and 1. Formula (22) is used to calculate the value:

$$LPSP = \sum_{t=1}^{24} \frac{P_{loss}(t)}{P_{load}(t)} \tag{22}$$

$P_{loss}(t)$ is calculated by following formula (Belboul, et al., 2022):

$$P_{loss}(t) = P_{load}(t) - \left[P_{WT}(t) + P_{PV}(t) + \eta P_{Bat}(t) + P_{DG}(t) \right] \qquad (23)$$

$$P_{WT}(t) = \sum_{i=1}^{N_{WT}} P_{WT-i}(t) \qquad (24)$$

$$P_{PV}(t) = \sum_{i=1}^{N_{PV}} P_{PV-i}(t) \qquad (25)$$

$$P_{Bat}(t) = \sum_{i=1}^{N_{Bat}} P_{Bat-i}(t) \qquad (26)$$

$$P_{DG}(t) = \sum_{i=1}^{N_{DG}} P_{DG-i}(t) \qquad (27)$$

$$N_i = (N_{WT}, N_{PV}, N_{Bat}, N_{DG}) \qquad (28)$$

Where, $P_{WT-i}(t)$ is the power generated by the i-th wind turbine at time t; $P_{PV-i}(t)$ represents the power generated by the i-th photovoltaic power generation at time t; $P_{Bat-i}(t)$ represents the power of the i-th battery at time t; $P_{DG-i}(t)$ represents the power generation of the i-th diesel generator at time t; N_i is the total number of the i-th device.

3.2.3 Environmental pollution index

The indicators of environmental pollution are expressed by the emissions and the difficulty of governance of CO_2, SO_2, and NO_x shown in Table 2. Equation (29) can be used to calculate the pollution index(Dong ,et al., 2021):

$$C_3 = \sum_{t=1}^{24} \left\{ \sum_{k=1}^{3} \left[\alpha_k \beta_k P_{DG}(t) \right] \right\} \qquad (29)$$

Where, C_3 is the environmental pollution index, k is the pollutant type, α_k is the pollution control standard coefficient, β_k is the pollutant emission coefficient, g/kW·h.

Table 2. Diesel generator pollution factors

Pollutant type (k)	β_k: Pollutant emission coefficient (g/kWh)	α_k: Pollution control standard coefficient
CO_2	649	0.21
SO_2	0.206	14.842
NO_x	9.89	62.964

3.2.4 Normalization coefficient of multi-objective function

When an independent micr-grid power supply configuration is faced with a complicated optimization decision problem among the economic objective, the power supply reliability objective, and the pollutant emission objective, it should be pursued to obtain the best power supply reliability level and lower environmental pollution index at a reasonable investment cost as the optimal trade-off decision result.

To improve the calculation speed of microgrid energy optimization, this paper simplifies the multi-objective function into a single objective function (comprehensive objective function C) through a series of proportional coefficients, which is solved by an

intelligent optimization algorithm, as shown in Equation(30) (Liu ,et al., 2022):

$$C = w_1 \cdot C_1 + w_2 \cdot C_2 + w_3 \cdot C_3 \tag{30}$$

Where, C is the comprehensive objective function. C_1 is the objective function of economic evaluation. C_2 is the objective function of reliability of the power supply. C_3 is the environmental pollution function. w_1, w_2 and w_3 are the proportions of C_1, C_2 and C_3 objective functions respectively.

3.3 Constraints

3.3.1 Real-time power balance

The installed capacities of PV, wind turbine, battery, and diesel generator should satisfy the demand-supply equality, as the following equations (31-33):

$$P_{load}(t) - P_{loss}(t) = P_{WT}(t) + P_{PV}(t) + P_{DG}(t) + \eta P_{Bat}(t) \tag{31}$$

$$\eta = \begin{cases} \eta_{discharge} & P_{Bat}(t) > 0 \\ \dfrac{1}{\eta_{charge}} & P_{Bat}(t) \leq 0 \end{cases} \tag{32}$$

$$P_{Bat}(t) = \begin{cases} P_{discharge}(t) & P_{Bat}(t) > 0 \\ P_{charge}(t) & P_{Bat}(t) \leq 0 \end{cases} \tag{33}$$

Where, $P_{load}(t)$is load power demand at time t, $P_{loss}(t)$ is deficit power at time t. P_{WT}, P_{PV}, P_{DG}, $P_{Bat}$are outpower at time t. η is the charging or discharging efficiency of the battery storage.

3.3.2 Battery characteristic Constraints

To extend the service life of the storage battery and reduce the replacement cost, some constraints are restricted as equations (34-35) (Liu, et al., 2017; Zhao ,et al., 2013):

$$SOC_{min} \leq SOC \leq SOC_{max} \tag{34}$$

Where, SOC_{min} is the limit under the battery capacity constraint, and SOC_{max} is the upper limit of the storage battery capacity. Meanwhile, to ensure the charging and discharging ability at the beginning, the initial value SOC(0) of the remaining electricity is set to 0.5.

$$\begin{cases} P_{charge}^{min} \leq P_{charge}(t) \leq P_{charge}^{max} \\ P_{discharge}^{min} \leq P_{discharge}(t) \leq P_{discharge}^{max} \end{cases} \tag{35}$$

Where, P_{charge}^{min}、 P_{charge}^{max}、 $P_{discharge}^{min}$、 $P_{discharge}^{max}$ are respectively the upper and lower limits of the battery charging and discharging power.

3.3.3 Maximum energy ratio between the diesel generator and load demand

The use of new energy generation should be given priority and the use of diesel engines should be minimized as much as possible. The maximum power supply ratio of diesel engine power generation is restricted as following equation (36) (Liu, 2021):

$$R_{DG} = \sum_{t=1}^{24} \left[\frac{P_{DG}(t)}{P_{load}(t)} \right] \le R_{DG\,max} \tag{36}$$

Where, $R_{DG\,max}$ is the maximum energy ratio, take it as 40%.

3.3.4 Loss of power supply probability (LPSP)

Due to the restriction in system output power and the growing load power demand, some demand is cut off to maintain the power balance. This cut-off power supply is limited as formula (37):

$$LPSP \le LPSP_{max} \tag{37}$$

where, $LPSP_{max}$ is the maximum value of LPSP, take it as 4%.

4. Optimization methods

Multi-objective optimizaition is a complex problem. Using meta-heuristic algorithms to solve this kind of problem can significantly improve the quality of solution results. This section gives a detailed introduction to the original WOA algorithm and the IWOA improvement process.

4.1 Whale optimization algorithm(WOA)

The whale optimization algorithm is a meta-heuristic optimization algorithm inspired by the hunting behavior of humpback whales (Mirjalili & Lewis, 2016). The WOA algorithm is inspired by this behavior and uses a spiral strategy to simulate the search method and rounding mechanism, which mainly includes the following three important stages (Watkins & Schevill, 1979).

Firstly, there is the stage of encircling prey whicn is expressed by the following formula (38-41):

$$\overline{X}(t+1) = \overline{X}^*(t) - \overline{A} \cdot \overline{D} \tag{38}$$

$$\overline{D} = \left| \overline{C} \cdot \overline{X}^*(t) - \overline{X}(t) \right| \tag{39}$$

$$\overline{A} = 2\overrightarrow{r_1} \cdot \overrightarrow{a} - \overrightarrow{a} \tag{40}$$

$$\overrightarrow{C} = 2\overrightarrow{r_2} \tag{41}$$

Where, $\overline{X}^*$ is the position vector of the best current whale individual, $\overline{X}$ is the position vector of the initialized whale individual, t represents the number of current iterations. $\overline{A}$ and $\overline{C}$ are coefficient vectors. $\overline{D}$ represents the distance vector between the current whale individual and the optimal whale individual. $\overrightarrow{a}$ represents a linearly decreasing vector from 2 to 0 throughout the iteration. $\overrightarrow{r_1}$ and $\overrightarrow{r_2}$ is a random vector distributed in between [0, 1].

Second, we have the stage of bubble net hunting: The position update between humpback whales and prey is expressed by a logarithmic spiral equation, as the following formula (42-43):

$$\overline{X}(t+1) = \overline{D}' \cdot e^{bl} \cdot \cos(2\pi l) + \overline{X}^*(t) \tag{42}$$

$$\overline{D}' = \left| \overrightarrow{X}(t) - \overrightarrow{X}^*(t) \right|$$ (43)

Where, b is the constant of the helix shape of the whale individual when it spirals forward, and when the value is 1, it is the ordinary logarithmic helix. l is the random number between [-1, 1]. $\overline{D}'$ is the distance vector between the search individual and the current optimal.

The WOA algorithm makes random selection according to probability p, and the position update formula is the following formula (44)：

$$\overline{X}(t+1) = \begin{cases} \overline{X}^*(t) - \overrightarrow{A} \cdot \overrightarrow{D} & p \leq 0.5 \\ \overline{D}' \cdot e^{bl} \cdot \cos(2\pi l) + \overrightarrow{X}^*(t) & p \geq 0.5 \end{cases}$$ (44)

Where , p is the probability of the predation mechanism and is the random number between [0, 1]. As the number of iterations increases, the parameters $\overline{A}$ and convergence factor $\vec{a}$ gradually decrease. If $\left| \overline{A} \right| < 1$, then all whales gradually surround the optimal current solution, which belongs to the local optimization stage in WOA.

Third, is the stage of searching prey: The mathematical model is as following formula (45-46):

$$\overline{X}(t+1) = \overline{X}_{rand}(t+1) - \overrightarrow{A} \cdot \overrightarrow{D}''$$ (45)

$$\overline{D}'' = \left| \overrightarrow{C} \cdot \overline{X}_{rand}(t) - \overline{X}(t) \right|$$ (46)

Where, $\overrightarrow{D}''$ is the distance vector between the current search individual and the random individual. $\overline{X}_{rand}(t)$ is the position vector of the random individual selected from the current population at the t-th iteration (random whale).

4.2 Improvement strategy

Adaptive t-distribution and differential mutation strategy are adopted to improve the WOA algorithm. Firstly, the adaptive t-distribution strategy is adopted to improve the whale bubble net predation method in the WOA algorithm when p>0.5; Secondly, the differential mutation strategy is used to perturb the algorithm when it falls into the optimal solution.

4.2.1 Adaptive t-distribution and dynamic selection strategy

This paper uses the t-distribution mutation operator with a degree-of-freedom parameter to perturb the whale position, The specific position update formula is as following equation (47):

$$\overline{X}(t+1) = \overline{X}(t) + \overline{X}(t) \cdot \overrightarrow{T}(t)$$ (47)

Where, $\overline{X}(t+1)$ is the position of the whale after a disturbance during the (t+1)-th iteration. $\overline{X}(t)$ is the position of the whale at the t-th iteration. The updated position $\overline{X}(t+1)$ is based on $\overline{X}(t)$ and adds a random interference term $\overline{X}(t) \cdot T(t)$, which not only fully utilizes the current position information but also adds random interference information.

Add the dynamic selection probability pp to adjust the use of the adaptive t-

distribution mutation operator, and its formula is as following equation (48):

$$pp = 1 - \frac{t_{max} - t}{t_{max}} \qquad (48)$$

Where, t_{max} is the maximum number of iterations, and t is the current number of iterations.

4.2.2 Differential variation perturbation strategy

Gaussian differencing can generate larger perturbations near the current mutated individual, making it easier to break out of the local extremum. The mathematical expression is as following equation (49)：

$$\overline{X}(t+1) = p_1 \cdot \left[\overrightarrow{X}^*(t) - \overline{X}(t) \right] + p_2 \cdot \left[\overrightarrow{X}_{rand}(t) - \overrightarrow{X}(t) \right] \qquad (49)$$

Where, $\overline{X}(t+1)$ is the position information of the disturbed whale. p_1 and p_2 are weight coefficients, both of which are random numbers with values of [0,1]. $\overrightarrow{X}^*(t)$ is the optimal location for the current whale. $\overrightarrow{X}(t)$ is the whale position information before disturbance. $\overrightarrow{X}_{rand}(t)$ provides location information for a random whale in the population.

4.3 IWOA flow chart

The IWOA algorithm flow chart of is shown in Figure 3.
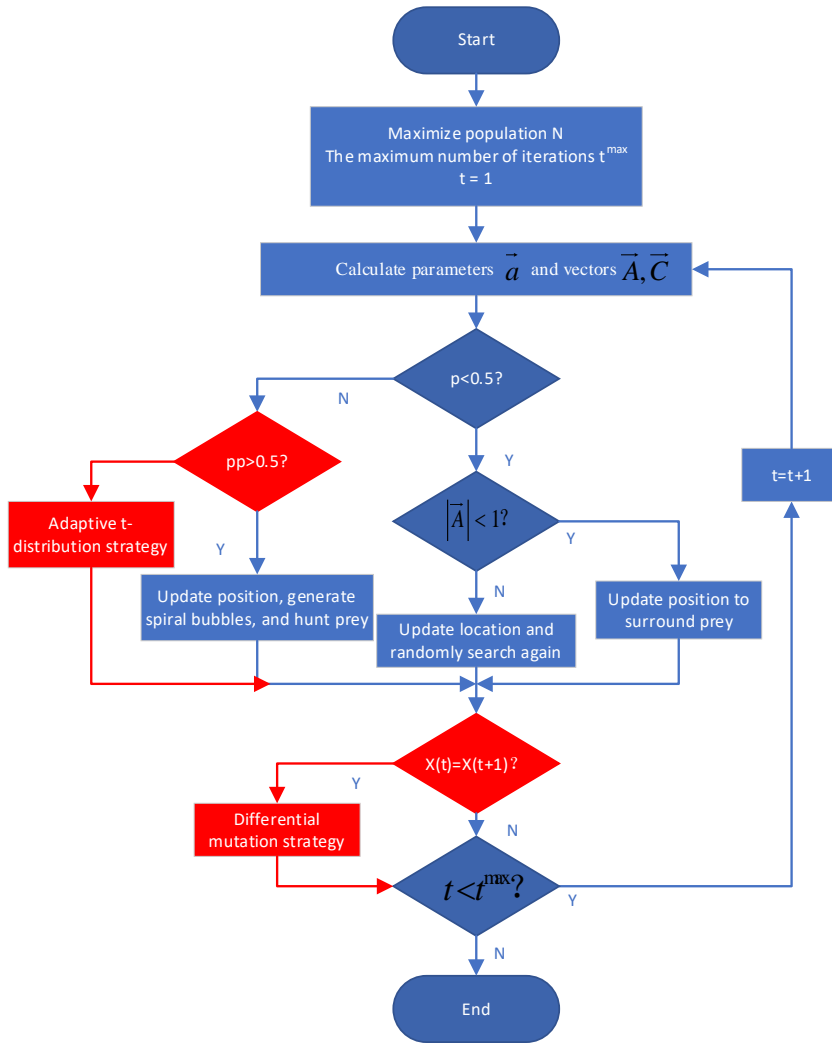
Figure 3. IWOA algorithm flowchart

4.4 Algorithm test

Some kinds of standard test functions used to test algorithms are listed in Table 3, and the test results are shown in Figure 4.

Table 3. Standard test functions

Function	Expression	Dim	F_{min}	Ranges
Unimodal	$F_1 = \sum_{i=1}^{N} x_i^2$	30	0	[-100, 100]
	$F_2 = \prod_{i=1}^{N} |x_i| + \sum_{i=1}^{N} |x_i|$	30	0	[-10, 10]
	$F_5 = \sum_{i=1}^{N} [100(x_{i+1} - x_i^2)^2 + (x_i - 1)^2]$	30	0	[-30, 30]
	$F_7 = \sum_{i=1}^{N} ix_i^4 + random[0,1)$	30	0	[-1.28, 1.28]
Multimodal		30	0	[-32, 32]

$$F_9 = -20 \times \exp(-0.2 \times \sqrt{\frac{1}{N}\sum_{i=1}^{N} x_i^2}) - \exp(\frac{1}{N}\sum_{i=1}^{N}\cos(2\pi x_i))$$
$$+20+e$$

$$F_{11} = \frac{\pi}{n}\left\{10\sin(\pi y_1) + \sum_{i=1}^{N-1} \begin{matrix}(y_i-1)^2[1+10\sin^2(\pi y_i+1)] \\ +(y_N+1)^2\end{matrix}\right\} \qquad 30 \qquad 0 \qquad [-50, 50]$$
$$+\sum_{i=1}^{N} u(x_i, 10, 100, 4)$$
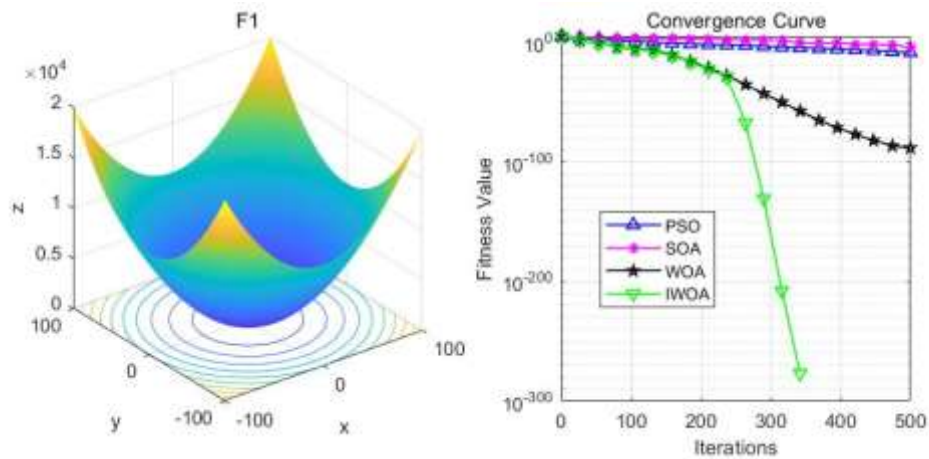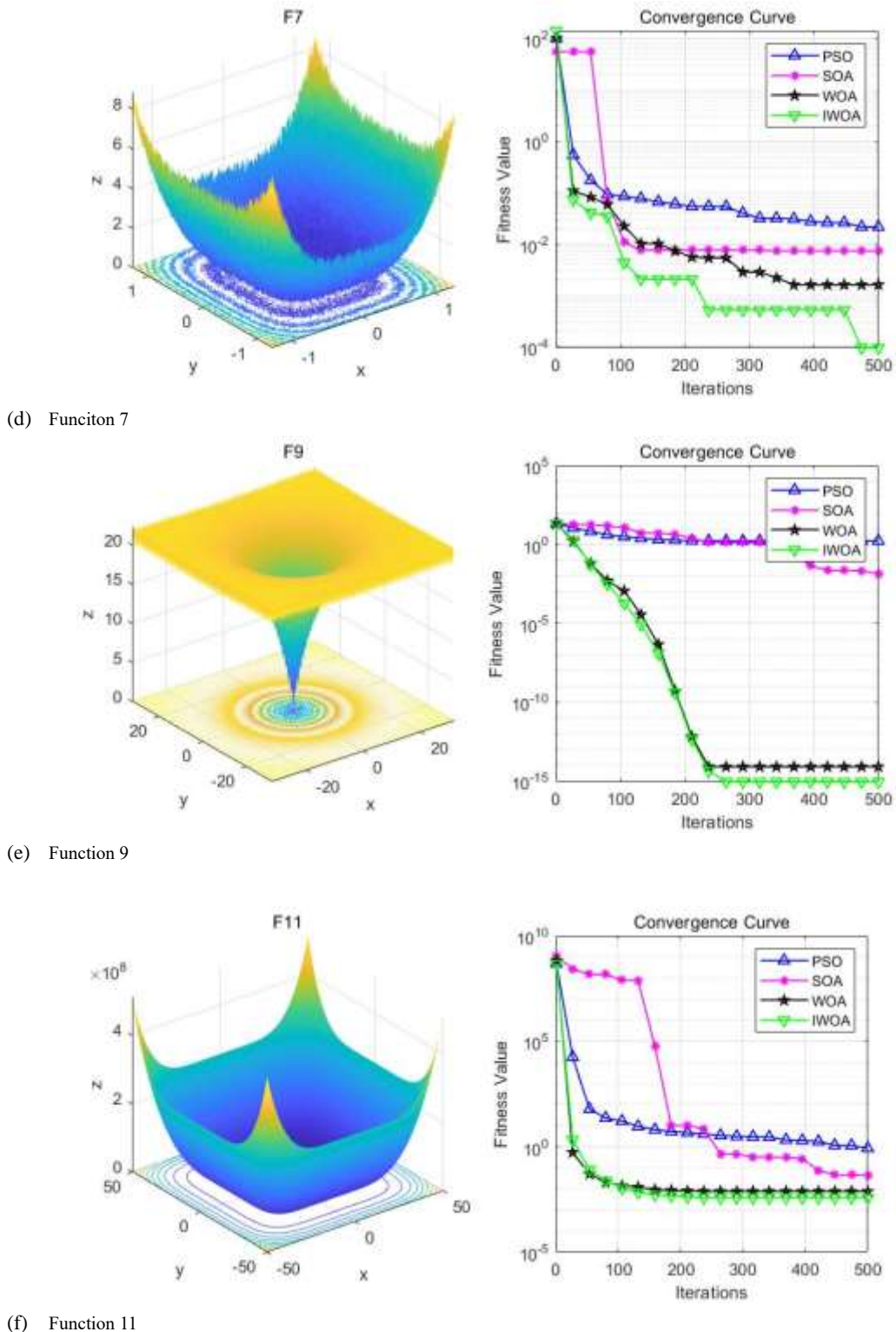

(a) Function 1

(b) Function 2

(c) Function 3

(d)   Funciton 7
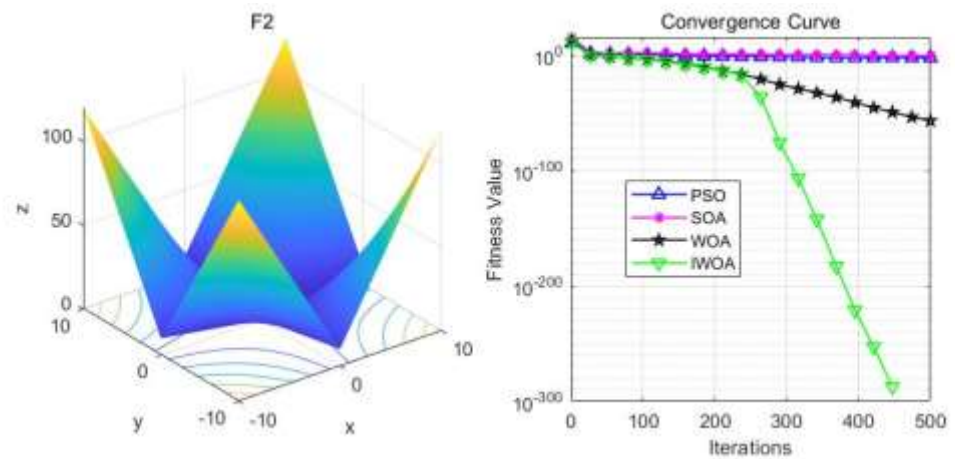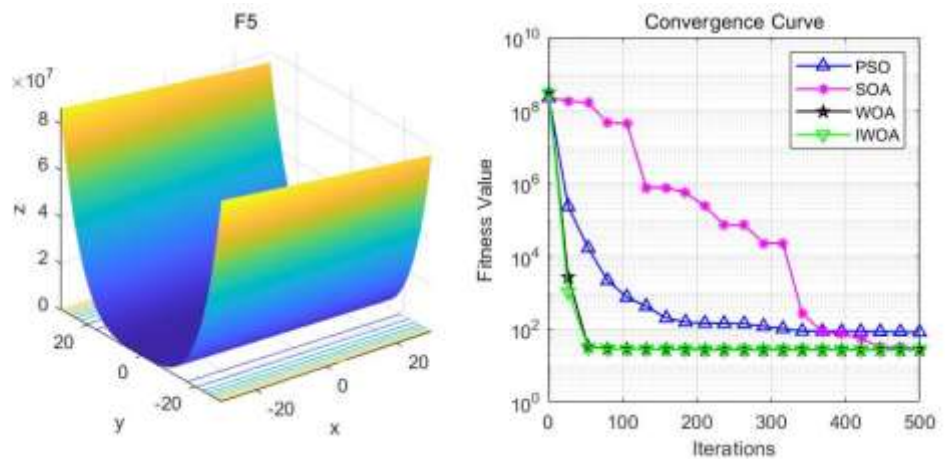
(e)   Function 9

(f)   Function 11

Figure 4. Three dimension diagraph and algorithm convergence curve of several function tests

5. Example analysis

To verify and study the supply capability of off-grid microgrid energy supply strategy and the solving ability of the IWOA algorithm, this study conducted a day-ahead scheduling

analysis of off-grid microgrid operation through the typical daily load data of a hospital complex in Montague, California, USA. The region experiences chilly winters characterized by relatively frequent snowfall, coupled with hot summers marked by significant diurnal temperature fluctuations and near-constant sunshine. The annual weather data and load power data are shown in Figures 5-8:
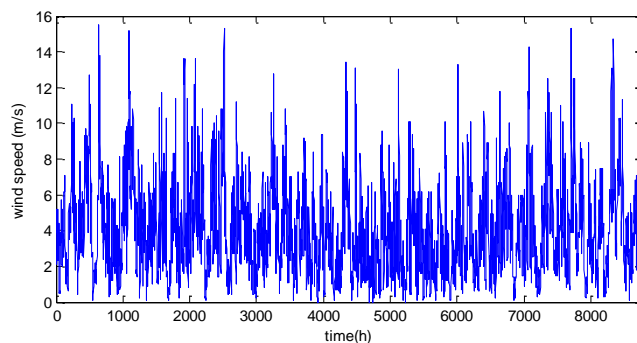
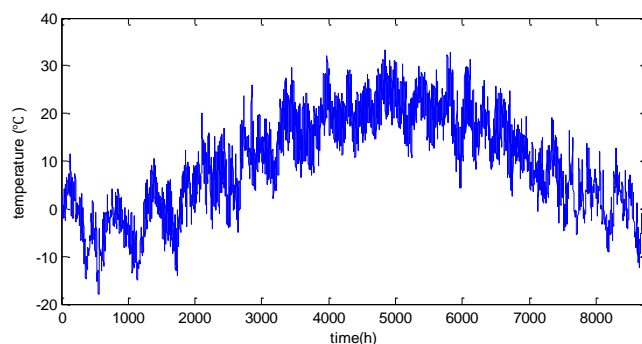**Figure 5.** Annual wind speed of the hospital
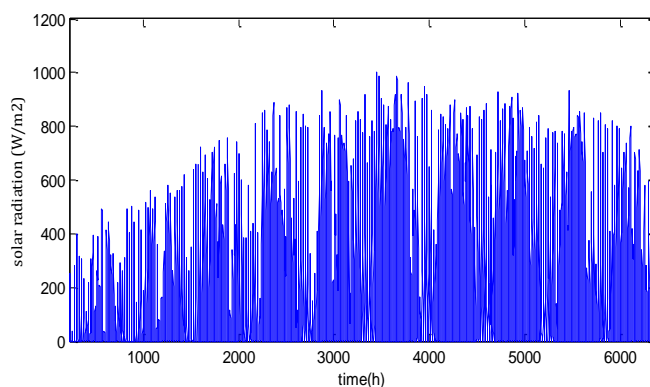
Figure 6. Annual solar radiation of the hospital

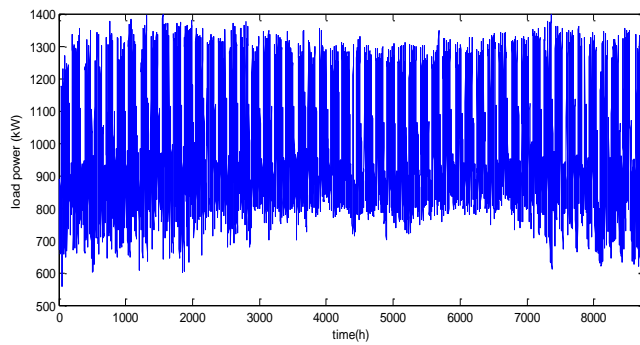
Figure 7. Annual temperature of the hospital

Figure 8. Annual load power of the hospital

The load profile studied is presented within the four seasons of the year—winter, spring, summer, and autumn. The optimization results of typical days in summer and winter were shown in Figure 9. Day-ahead economic scheduling is divided into 24 decision stages (24 hours), each decision interval 1h. Load forecasting is carried out according to the pre-day load data, and the new energy generation of wind power generation and photovoltaic power generation is predicted through the weather data.
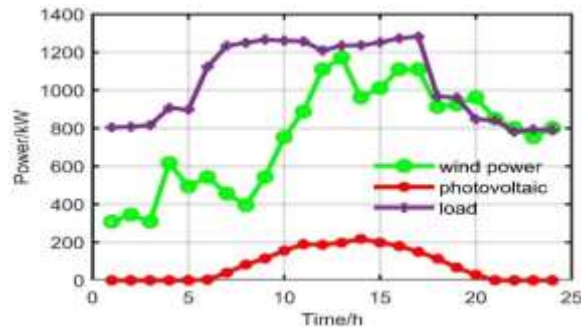
(a)   summer
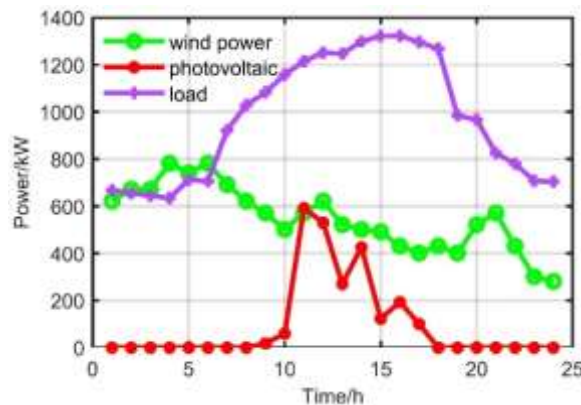
(b)   winter

Figure 9. Comparison of new energy output and load demand

On a typical summer day, as shown in Figure 9(a), the load demand fluctuates from 789-1281 kW, showing the overall characteristics of "high load during the day and low load at night"; The volatility of wind power generation is strong, its output power is no more than 600 kW from 1 to 10 o 'clock, and increases from 394 kW to 1109 kW rapidly from 8 to 12 o 'clock, then shows a fluctuation decline before 24 o 'clock, and the output power is about 800 kW at 24 o 'clock; Photovoltaic power generation works from 6 to 21 o'clock only, the

output power increases to 189 kW at 11 o 'clock, the highest value is 217 kW at 14:00, then continues to be about 200 kW before 15 o 'clock, and then decrease to 0 at 21 o'clock. In Figure 9(b), the wind turbine output power is below 800 kW whole day, the photovoltaic power is upper 200 kW during 10-15 o'clock.

The wind-solar hybrid power system includes wind turbines, photovoltaic power generation, energy storage batteries, and diesel generators. The specific parameters of the equipment are shown in Table 4.

Table 4. Technical parameters of distributed generator and energy storage battery

distribute generator	parameters	symbols	value
wind turbine	Cut in wind speed	v_i(m/s)	2.5
	Rated wind speed	v_r(m/s)	12
	Cut out wind speed	v_P(m/s)	18
	Rated power	P_{WTr}(kW)	20
	Unit cost	C_{WT} (¥/set)	90700
	Unit O&M cost	C_{OMWT} (¥/kW)	0.06
photovoltaic	Rated power	P_{PVr}(kW)	20
	Unit cost	C_{PV}(¥/set)	100000
	Unit O&M cost	C_{OMPV}(¥/kW)	0.04
energy storage battery	Capacity	E_{Bat} (kWh)	5
	Self-discharge rate	δ(%/h)	2
	Charging efficiency	η_{charge}(%)	95
	Discharge efficiency	$\eta_{discharge}$(%)	95
	Rated power	P_{Batr}(kW)	2.5
	Minimum state of charge	SOCmin	0.1
	Maximum state of charge	SOCmax	0.9
	Unit cost	C_{Bat}(¥/set)	7835
	Unit O&M cost	C_{OMBat}(¥/kWh)	0.16
diesel generator	Rated power	P_{DGr} (kW)	10
	Intercept coefficient	c_{f1}	0.0845
	Curve slope	c_{f2}	0.245
	Diesel unit price	U_{fuel} (¥/L)	6.11
	Unit cost	C_{DG}(¥/set)	12830
	Unit O&M cost	C_{OMDG}(¥/kW)	0.04

5.1 IWOA algorithm test results

After multiple instance simulation tests, the IWOA has significant advantages in algorithm convergence speed and accuracy by comparing with PSO (Kennedy & Eberhart, 1995; Zhan, et al., 2009), WOA, and SOA(Dhiman & Kumar, 2019), it shows better computational performance in the examples presented in this paper, and the effect diagram is shown in Figure 10.
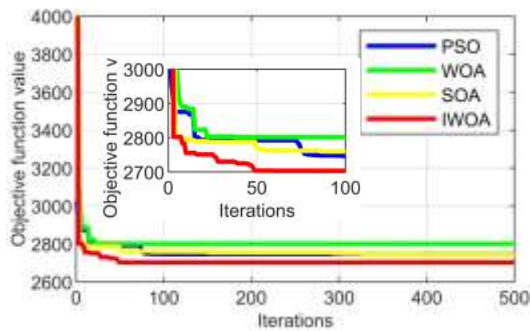
(a)　summer
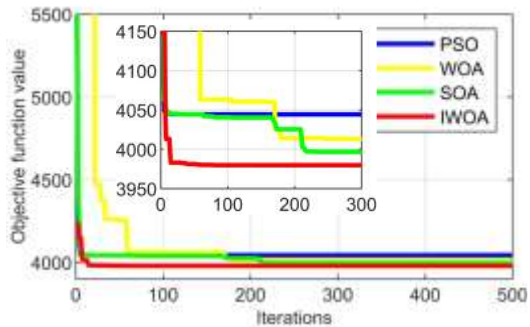
(b)　winter

Figure 10. Iterative convergence diagram

Figure 10(a) is the iterative convergence diagram of summer typical day, the optimal solutions and the number of iterations that converge to the optimal solution earliest of the PSO algorithm, the WOA algorithm, the SOA algorithm, and the IWOA algorithm are shown in Table 5. The algorithm response to the number of wind turbines, photovoltaic panels, diesel generators, and batteries in the optimal solution is shown in Table 6. Figure 10(b) is the iterative convergence diagram of winter typical day. The results for typical day in winter are basically the same as in summer, no additional analysis will be done in this paper.

Table 5. Algorithm Iteration Convergence Table

algorithm	Optimal solution	Convergence times
PSO	2743	86
WOA	2801	38
SOA	2745	82
IWOA	2703	49

Table 6. Optimization Results of Microgrid Capacity

| algorithm \ types	WT	PV	DG	Bat
PSO	60	12	78	100
WOA	60	11	80	76
SOA	59	14	98	92
IWOA	59	15	77	77

5.2 Operating efficiency of new energy equipment

The working state of the wind and photovoltaic power generation is simplified as a

proportional relationship 0-1 as shown in Figure 11, where 0 represents the stopping operation of the equipment and 1 represents the equipment running at full load.
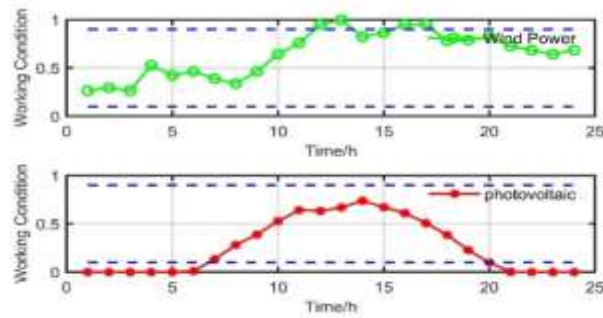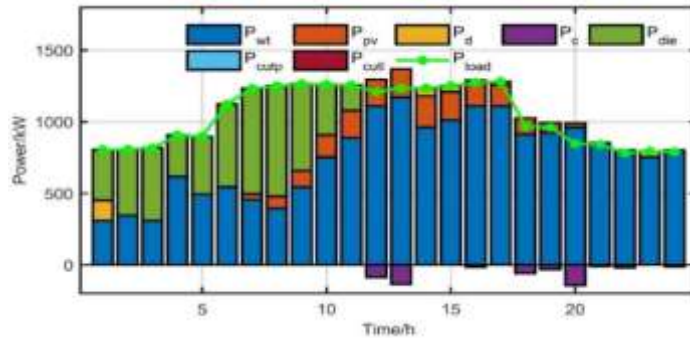

(a)   summer
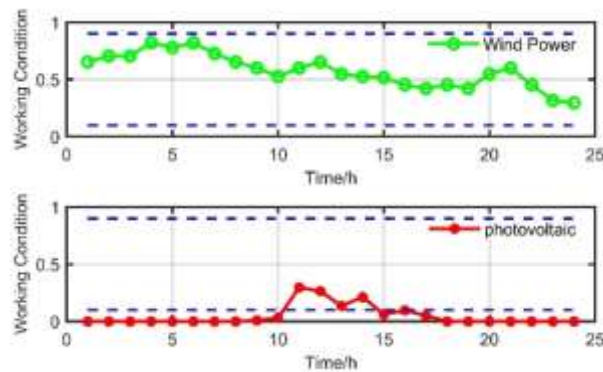
(b)   winter

**Figure 11.** Working condition diagram of new energy equipment

Figure 11(a) is the working condition diagram of new energy equipment in summer, Figure 11(b) is the working condition diagram of new energy equipment in winter. Analysis with the typical summer day, It can be seen that both wind turbines and photovoltaics have achieved optimal utilization rates. The utilization rate of wind turbines exceeds 50% during 10-24 o'clock, exceeds 90% in periods of 12-13 o'clock and 16-17 o'clock, and operates at maximum utilization rate at 13 o'clock. The utilization rate of photovoltaic power generation reaches 64.22% at 11 o'clock, reaches its highest point of 73.82% at 14:00 and exceeds 50% during 10- 17 o'clock.

5.3 Output situation
Based on the energy supply strategy and the IWOA algorithm, the output power of each type of equipment in each period is shown in Figure 12:
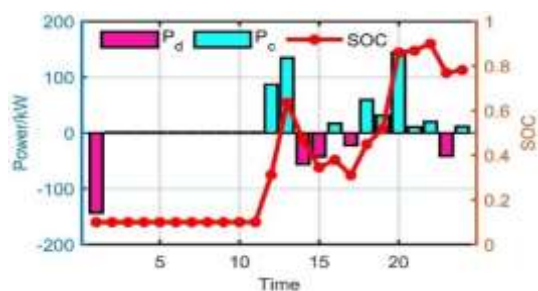
(a)　summer
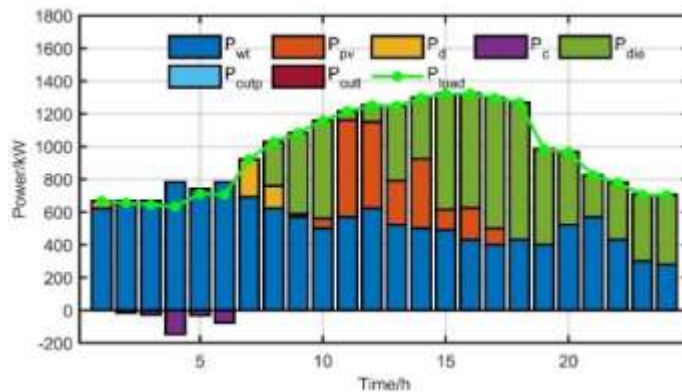
(b)　winter

Figure 12. Microgrid energy balance diagram

Analysis with the typical summer day, in Figure 12(a), during 1-11 o'clock the new energy output cannot meet the load demand at, and the auxiliary role of batteries and diesel is needed to meet the power balance of the microgrid, the output power of diesel generators accounts for almost half of the load sometime, its output power reaches its maximum value 772 kW at 8 o'clock. Power balance is achieved through wind power generation, photovoltaic power generation, and the auxiliary role of batteries during 12:00 -24:00, with wind power generation accounting for more than 90% of load demand. The load demand is primarily met by wind turbines. The charging period of the battery is mainly concentrated in 12-13 o'clock, 16 o'clock, 18-22 o'clock, etc. In both (a) and (b), the power cut and the load cut in the system are both 0, indicating that there is no situation in the microgrid where the load demand cannot be met or the output of new energy cannot be consumed during the entire period of a typical day.

5.4 Operation of energy storage battery
Energy storage is charged when the output of new energy equipment exceeds the load demand and discharged when the output of new energy equipment is less than the load demand. Based on the output power of various devices in Figure 13, the charging and discharging power and SOC state of energy storage are analyzed.

(a) summer
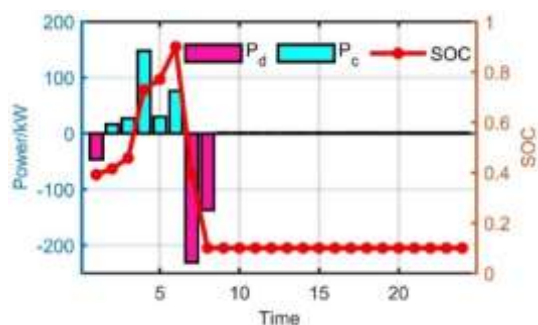
(b) winter

Figure 13. Working state of the energy storage battery

Analysis with the typical summer day, in Figure 13(a), considering that the new energy output at 1 o'clock is less than the load demand, the discharge power of the battery is 143 kW. After discharge, the SOC state of the battery drops to the lower limit of safe operation 0.1. From 1 to 11 o'clock, the SOC remains at 0.1. After charging from 11 to 12 o'clock, the SOC reached 0.635, and then it went through a discharge state, dropping to 0.316 at 17 o'clock. At 18-22 o'clock, the battery is in a charging state, and the charging power reaches its upper limit at 20 o'clock, which is 143 kW. At 22 o'clock, the SOC reaches its highest state, which is 0.9. In Figure 12(b), battery charging and discharging is mainly concentrated in 0-8 o'clock. The optimal safe operating state of the battery has a SOC fluctuation range of 0.1-0.9.

The working conditions of each distributed generator are listed according the above analysis in Table 7.

Table 7 The distributed generators' working conditions at each sampling time

Time(h)	WT	PV	DE	Bat		Working State
1	Full	—	Tracking load	$P_{discharge}^{max}$		4
2	Full	—	Tracking load	—		3
3	full	—	Tracking load	—		3
4	Full	—	Tracking load	—		3
5	Full	—	Tracking load	—		3
6	Full	—	Tracking load	—		3
7	Full	Full	Tracking load	—		3
8	Full	Full	Full	—		2
9	Full	Full	Tracking load	—		3
10	Full	Full	Tracking load	—		3
11-	Full	Full	Tracking load	—		3
12	Full	Full	—	Tracking load(charge)		5
13	Full	Full	—	Tracking load(charge)		5

Time(h)	WT	PV	DE	Bat	Working State
14	Full	Full	—	Tracking load(discharge)	6
15	Full	Full	—	Tracking load(discharge)	6
16	Full	Full	—	Tracking load(charge)	6
17	Full	Full	—	Tracking load(discharge)	6
18	Full	Full	—	Tracking load(charge)	6
19	Full	Full	—	Tracking load(charge)	6
20	Full	Full	—	P_{charge}^{max}	7
21	Full	—	—	Tracking load(charge)	6
22	Full	—	—	Tracking load(charge)	8
23	Full	—	—	Tracking load(discharge)	6
24	Full	—	—	Tracking load(charge)	6

The working state is mostly in normal 3, 4, 5, and 6 states, indicating that the final capacity obtained based on the constructed microgrid model and the IWOA algorithm can meet the load requirements of the design object while avoiding situations such as wind and solar power abandonment.

6. Conclusion and contribution

This paper constructs an energy scheduling strategy that prioritizes the use of new energy generation equipment output under an energy storage priority control strategy based on diesel generator turn-on/off conditions. Then the WOA algorithm is improved through adaptive t-distribution, dynamic selection strategy, and differential mutation strategy. Aiming at the operational characteristics of off-grid microgrids, a multi-objective optimization function was constructed with the number of power generation and energy storage equipment as optimization variables, which simultaneously considers economic, reliability, and environmental protection. Compared with the PSO algorithm, SOA algorithm, and WOA algorithm, the IWOA algorithm obtains the optimal result when solving, with a comprehensive objective function of 2702 yuan. The algorithm converges in the 49th iteration.

After verification, the energy scheduling strategy constructed in this study effectively solves the energy scheduling problem of off-grid microgrids. , which improves the original algorithm's poor solving accuracy and susceptibility to local convergence, and improves the solving speed and optimization accuracy.

As part of future work, consider diversifying some other clean energy sources such as biomass and geothermal energy, tidal energy, etc. in line with the capabilities of each region. Another perspective is considering the integration and transformation of multiple load demands, such as the cooling and heating load demand.

Authors Contributions:

Conceptualization, Jia Lu; Data curation, Jia Lu; Formal analysis, Fei Lu Siaw and Tzer Hwai Gilbert Thio; Investigation, Jia Lu; Methodology, Jia Lu and Jun Jie Wang; Project administration, Jia Lu and Fei Lu Siaw; Resources, Jun Jie Wang; Software, Jun Jie Wang; Supervision, Fei Lu Siaw and Tzer Hwai Gilbert Thio; Validation, Dong Yang;

Visualization, Jun Jie Wang; Writing – original draft, Jia Lu; Writing – review & editing, Jia Lu, Fei Lu Siaw and Tzer Hwai Gilbert Thio.

All authors have read and agreed to the published version of the manuscript.

Corresponding author: Jia Lu; Fei Lu Siaw

Conflicts of Interest:

The authors declare no conflict of interest.

Data Availability section:

The data in paper can be download at Open Energy Data Initiative (OEDI), the link is https://data.openei.org/submissions/153

Funding Declaration: This study did not receive any funding in any form.

References:

[1]Abdalla, A. N., Nazir, M. S., Tao, H., Cao, S., Ji, R., Jiang, M., & Yao, L. (2021). Integration of energy storage system and renewable energy sources based on artificial intelligence: An overview. Journal of Energy Storage, 40, 102811.

[2]Aeidapu MAHESH, K. S. S. (2020). A genetic algorithm based improved optimal sizing strategy for solar-wind-battery hybrid system using energy filter algorithm. Front. Energy, 14(1), 139-151.

[3]Akbas, B., Kocaman, A. S., Nock, D., & Trotter, P. A. (2022). Rural electrification: An overview of optimization methods. Renewable and Sustainable Energy Reviews, 156.

[4]Akikur, R. K., Saidur, R., Ping, H. W., & Ullah, K. R. (2013). Comparative study of stand-alone and hybrid solar energy systems suitable for off-grid rural electrification: A review. Renewable and Sustainable Energy Reviews, 27, 738-752.

[5]Amupolo, A., Nambundunga, S., Chowdhury, D. S. P., & Grün, G. (2022). Techno-economic feasibility of off-grid renewable energy electrification schemes: a case study of an informal settlement in Namibia. Energies, 15(12).

[6]Bakeer, A., Elmorshedy, M. F., Salama, H. S., Elkadeem, M. R., Almakhles, D. J., & Kotb, K. M. (2023). Optimal design and performance analysis of coastal microgrid using different optimization algorithms. Electrical Engineering, 105(6), 4499-4523.

[7]Belboul, Z., Toual, B., Kouzou, A., Mokrani, L., Bensalem, A., Kennel, R., & Abdelrahem, M. (2022). Multiobjective Optimization of a Hybrid PV/Wind/Battery/Diesel Generator System Integrated in Microgrid: A Case Study in Djelfa, Algeria. Energies, 15(10).

[8]Bukar, A. L., Tan, C. W., Yiew, L. K., Ayop, R., & Tan, W.-S. (2020). A rule-based energy management scheme for long-term optimal capacity planning of grid-independent microgrid optimized by multi-objective grasshopper optimization algorithm. Energy Conversion and Management, 221, 113161.

[9]Chen, X., Xiao, J., Yuan, J., Xiao, Z., & Gang, W. (2021). Application and performance analysis of 100% renewable energy systems serving low-density communities. Renewable Energy, 176, 433-446.

[10]Chunhui Liang, C. D., Xiaoyang Zuo, Jinfa Li, Qing Guo. (2023). Capacity configuration optimization of wind-solar combined power generation system based on improved grasshopper algorithm. Electric Power Systems Research, 109770-109782.

[11]Das, B. K., Hoque, N., Mandal, S., Pal, T. K., & Raihan, M. A. (2017). A techno-economic

feasibility of a stand-alone hybrid power generation for remote area application in Bangladesh. Energy, 134, 775-788.

[12]Dhiman, G., & Kumar, V. (2019). Seagull optimization algorithm: Theory and its applications for large-scale industrial engineering problems. Knowledge-Based Systems, 165, 169-196.

[13]Dong, J., Dou, Z., Si, S., Wang, Z., & Liu, L. (2021). Optimization of capacity configuration of wind–solar–diesel–storage using improved sparrow search algorithm. Journal of Electrical Engineering & Technology, 17(1), 1-14.

[14]Emad, D., El-Hameed, M. A., & El-Fergany, A. A. (2021). Optimal techno-economic design of hybrid PV/wind system comprising battery energy storage: Case study for a remote area. Energy Conversion and Management, 249.

[15]International Energy Agency. (2023). Renewables 2022/Analysis and forecasts to 2027. www.iea.org/corrections

[16]Kennedy, J., & Eberhart, R. (1995, 27 Nov.-1 Dec. 1995). Particle swarm optimization. Paper presented at the Proceedings of ICNN'95 - International Conference on Neural Networks.

[17]Kotb, K. M., Elmorshedy, M. F., Salama, H. S., & Dán, A. (2022). Enriching the stability of solar/wind DC microgrids using battery and superconducting magnetic energy storage based fuzzy logic control. Journal of Energy Storage, 45, 103751.

[18]Lian, J., Zhang, Y., Ma, C., Yang, Y., & Chaima, E. (2019). A review on recent sizing methodologies of hybrid renewable energy systems. Energy Conversion and Management, 199, 112027.

[19]Liang, C., Ding, C., Zuo, X., Li, J., & Guo, Q. (2023). Capacity configuration optimization of wind-solar combined power generation system based on improved grasshopper algorithm. Electric Power Systems Research, 225.

[20]Liu, C., Wang, X., Wu, X., & Guo, J. (2017). Economic scheduling model of microgrid considering the lifetime of batteries. IET Generation, Transmission & Distribution, 11(3), 759-767.

[21]Liu, H. (2021). Research on multi-objective optimal capacity configuration for stand-alone microgrid with WT-PV-DE-BES. Inner Mongolia University of Technology,

[22]Liu, Y., Yang, S., Li, D., & Zhang, S. (2022). Improved Whale Optimization Algorithm for Solving Microgrid Operations Planning Problems. Symmetry, 15(1).

[23]Małgorzata Wiatros-Motyka. (2023). Global Electricity Review 2023. https://ember-climate.org/insights/research/global-electricity-review-2023/#supporting-material

[24]Mirjalili, S., & Lewis, A. (2016). The Whale Optimization Algorithm. Advances in Engineering Software, 95, 51-67.

[25]Rajanna, S., & Saini, R. P. (2016). Development of optimal integrated renewable energy model with battery storage for a remote Indian area. Energy, 111, 803-817.

[26]Shezan, S. A., Kamwa, I., Ishraque, M. F., Muyeen, S. M., Hasan, K. N., Saidur, R., Rizvi, S. M., Shafiullah, M., & Al-Sulaiman, F. A. (2023). Evaluation of Different Optimization Techniques and Control Strategies of Hybrid Microgrid: A Review. Energies, 16(4).

[27]Watkins, W. A., & Schevill, W. E. (1979). Aerial observation of feeding behavior in four baleen whales: eubalaena glacialis, balaenoptera borealis, megaptera novaeangliae, and balaenoptera physalus. Journal of Mammalogy, 60(1), 155-163.

[28]Yoshida, Y., & Farzaneh, H. (2020). Optimal Design of a Stand-Alone Residential Hybrid Microgrid System for Enhancing Renewable Energy Deployment in Japan. Energies, 13(7).

[29]Zhan, Z., Zhang, J., Li, Y., & Chung, S. (2009). Adaptive particle swarm optimization. IEEE Transactions on Systems Man, and Cybernetics — Part B: Cybernetics, 39(6), 1362-1381.

[30]Zhao, B., Zhang, X., Chen, J., Wang, C., & Guo, L. (2013). Operation Optimization of Standalone Microgrids Considering Lifetime Characteristics of Battery Energy Storage System. IEEE Transactions on Sustainable Energy, 4(4), 934-943.

[31]Zhao, J., & Yuan, X. (2016). Multi-objective optimization of stand-alone hybrid PV-wind-diesel-battery system using improved fruit fly optimization algorithm. Soft Computing, 20(7), 2841-2853.

[32]Zhao, Y., Liu, Y., Wu, Z., Zhang, S., & Zhang, L. (2023). Improving Sparrow Search Algorithm for Optimal Operation Planning of Hydrogen–Electric Hybrid Microgrids Considering Demand Response. Symmetry, 15(4).